

## Light-by-light scattering in ultraperipheral collisions of heavy ions at two future detectors

Paweł Jucha<sup>1,\*</sup>, Mariola Klusek-Gawenda<sup>1,†</sup> and Antoni Szczurek<sup>1,2,‡</sup>

<sup>1</sup>*Institute of Nuclear Physics Polish Academy of Sciences,  
ul. Radzikowskiego 152, PL-31-342 Kraków, Poland*

<sup>2</sup>*College of Mathematics and Natural Sciences, University of Rzeszów,  
ul. Pigonia 1, PL-35-310 Rzeszów, Poland*



(Received 22 August 2023; accepted 22 November 2023; published 3 January 2024)

We discuss possible future studies of photon-photon (light-by-light) scattering using a planned FoCal and ALICE 3 detectors. We include different mechanisms of  $\gamma\gamma \rightarrow \gamma\gamma$  scattering such as double-hadronic photon fluctuations,  $t/u$ -channel neutral pion exchange or resonance excitations ( $\gamma\gamma \rightarrow R$ ) and deexcitation ( $R \rightarrow \gamma\gamma$ ). The broad range of (pseudo)rapidities and lower cuts on transverse momenta open a necessity to consider not only dominant box contributions but also other subleading contributions. Here we include low mass resonant  $R = \pi^0, \eta, \eta'$  contributions. The resonance contributions give intermediate photon transverse momenta. However, these contributions can be eliminated by imposing windows on diphoton invariant mass. We study and quantify individual box contributions (leptonic, quarkish). The electron/positron boxes dominate at low  $M_{\gamma\gamma} < 1$  GeV diphoton invariant masses. The  $\text{PbPb} \rightarrow \text{PbPb}\gamma\gamma$  cross section is calculated within equivalent photon approximation in the impact parameter space. Several differential distributions are presented and discussed. We consider four different kinematic regions. We predict a cross section in the (mb-b) range for typical ALICE 3 cuts, a few orders of magnitude larger than for the current ATLAS or CMS experiments. We also consider the two- $\pi^0$  background which can, in principle, be eliminated at the new kinematical range for the ALICE 3 measurements by imposing dedicated cuts on diphoton transverse momentum and/or so-called vector asymmetry.

DOI: 10.1103/PhysRevD.109.014004

### I. INTRODUCTION

The photon-photon scattering, often called light-by-light scattering, is an interesting quantum effect. Till recently, it was not studied experimentally. It was a dream for the laser community. The works in this direction by the laser community are going on [1]. The possibility of light-by-light studies in ultraperipheral heavy ion collisions (UPC) was proposed in [2]. Inspired by the theoretical analyses it was then studied experimentally by the ATLAS [3] and CMS [4] collaborations. Statistics improved data were presented in [5,6]. The experimental data can be almost explained taking into account only QED box contributions. The ATLAS and CMS measurements can register only transverse momenta of photons larger than about

2–2.5 GeV, i.e., automatically large diphoton masses. As matter of course, this means small statistics of several tens of events. It was discussed in [7] what the ALICE and LHCb collaborations could do for smaller diphoton invariant masses. According to our knowledge, the experimental analysis of the ALICE collaboration is in progress. The previous studies of nuclear reactions considered almost exclusively so-called box contributions. Other underlying mechanisms were discussed rather only for  $\gamma\gamma \rightarrow \gamma\gamma$  scattering in [7–10]. The authors of [11] considered also diffractive mechanisms of production of two photons associated however with extra hadronic emissions. The  $\gamma\gamma \rightarrow \gamma\gamma$  is also interesting in the context of searching for effect beyond the Standard Model [12].

In this analysis, we explore what future FoCal [13] and ALICE 3 [14] detectors could do in this respect. A forward electromagnetic calorimeter is planned as an upgrade to the ALICE experiment for data taking in 2027–2029 at the LHC. The FoCal will cover pseudorapidities range of  $3.4 < \eta < 5.8$ . Runs 5 and 6 will allow to measure more than five times the present Pb-Pb luminosity. This increase of luminosity, in combination with improved detector capabilities, will enable the success of the physical program planned in ALICE 3.

\*Pawel.Jucha@ifj.edu.pl

†Mariolola.Klusek@ifj.edu.pl

‡Antoni.Szczurek@ifj.edu.pl

*Published by the American Physical Society under the terms of the Creative Commons Attribution 4.0 International license. Further distribution of this work must maintain attribution to the author(s) and the published article's title, journal citation, and DOI. Funded by SCOAP<sup>3</sup>.*

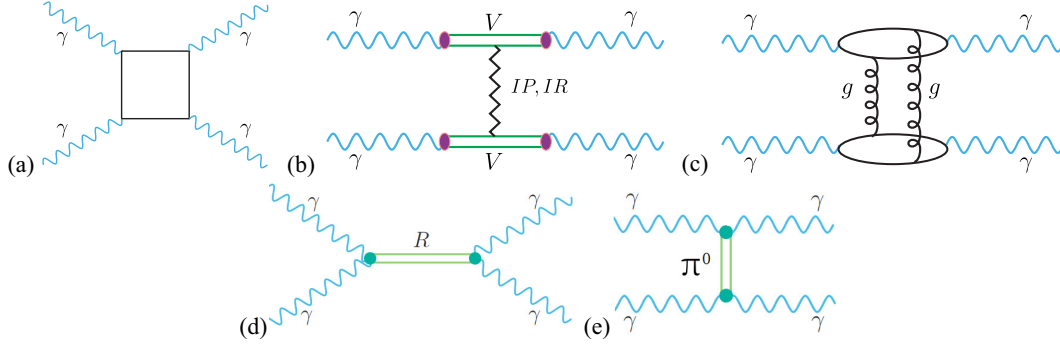


FIG. 1. Feynman diagrams of the mechanism: (a) fermionic loop, (b) VDM-Regge contribution, (c) 2-gluon exchange, (d) low mass resonances in the  $s$  channel, (e)  $\pi^0$  resonance in the  $t$  channel.

A significant feature of FoCal and ALICE 3 programs is the ability to measure photons in relatively low (starting from a few MeV) transverse momenta.

In the present paper we will consider not only box contributions but also contributions of the other mechanisms (double photon hadronic fluctuations,  $\pi^0$   $t/u$ -channel exchanges, two-gluon exchange, etc.). We will explore whether the other mechanisms that are less under theoretical control (nonperturbative pQCD domain), can be observed experimentally with the future apparatus. We will try to find conditions how to relatively enhance them compared to the box contributions to be observed in heavy ion UPC.

## II. SKETCH OF THE FORMALISM

### A. Elementary cross section and general remarks

The Weizsäcker-Williams formula (see Sec. II C) is based on the knowledge of the elementary  $\gamma\gamma \rightarrow \gamma\gamma$  cross section. The angular distribution of  $\gamma\gamma \rightarrow \gamma\gamma$  depends on  $z = \cos(\theta)$  where  $z$  is in range  $(-1, 1)$ , and  $\theta$  is the scattering angle, and the mass of the particles produced in the process  $M_{\gamma\gamma}$ . Determination of the elementary cross section requires a calculation of photon-photon scattering amplitudes derived from Feynman diagrams of fermionic loops [Fig. 1(a)]. As shown in [9], higher-order processes such as vector dominance model (VDM)-Regge [Fig. 1(b)] and 2-gluon exchanges [Fig. 1(c)] can be important at energies above 30 GeV, while in the low-energy regime, these processes should not play a significant role.

The first diagram is an example of a standard box diagram, the second diagram corresponds to double photon hadronic fluctuations and will be called the VDM-Regge contribution due to the way the model is formulated. It can be calculated reliably for  $|\hat{t}|, |\hat{u}| \ll \hat{s}$ . The third diagram is an example of the two-gluon exchanges. From a formal point of view, it is an example of a class of three-loop diagrams. Its contribution can be calculated/estimated easily at “high-energy” the energy is much higher than

the constituent quark masses and not too small transverse momenta where there is a double-counting with the VDM-Regge contribution [7]. The fourth diagram is an example of  $\pi^0$  exchanges, not explicitly included in the VDM-Regge approach [15]. It can be reliably calculated down to a small  $\gamma\gamma \rightarrow \gamma\gamma$  collision energies.

Only the first two mechanisms will be discussed here in a more detailed way. We will show that the contribution of the third and fourth diagrams, discussed in [7,15], will be very small, practically negligible for the considered range of kinematics ( $W_{\gamma\gamma}, \cos\theta^*$ ).

Future theoretical studies would require a systematic approach to three-loop calculations. This goes beyond the scope of the present paper.

The distribution of the elementary cross section for low energies is known and has been shown at least in [8], but so far, no one has used this for light-by-light scattering calculation below 5 GeV due to experimental limitations. Moreover, this is the first paper where the influence of the different types of particles generated in the loop on total cross section is shown explicitly.

In the present work, the minimum mass of invariant produced photons is 10 MeV, which, according to the formula  $p_{t,\min} = M_{\min}/2$ , means that the minimum value of the transverse momentum can be 5 MeV. The elementary cross section here is calculated for unpolarized photons. To do this, all 16 photon helicity combinations of the cross section/amplitude must be added up. In fact, due to symmetries, it is sufficient to count only five combinations and then add them up with the corresponding weights:

$$\sum_{\lambda_1, \lambda_2, \lambda_3, \lambda_4} |\mathcal{A}_{\lambda_1 \lambda_2 \rightarrow \lambda_3 \lambda_4}^{\gamma\gamma \rightarrow \gamma\gamma}|^2 = 2|\mathcal{A}_{++++}^{\text{fermions}}|^2 + 2|\mathcal{A}_{+---}^{\text{fermions}}|^2 + 2|\mathcal{A}_{+--+}^{\text{fermions}}|^2 + 2|\mathcal{A}_{-++-}^{\text{fermions}}|^2 + 8|\mathcal{A}_{++++}^{\text{fermions}}|^2. \quad (2.1)$$

Elementary cross section calculations for the box contribution were carried out using FormCalc and LoopTools libraries based on *Mathematica* software.

### B. Double-photon hadronic fluctuations

This component was calculated for the first time in [8,9] assuming vector dominance model. In this approach, the amplitude for the process is given as

$$\begin{aligned} \mathcal{M} = & \Sigma_{i,j} C_i^2 C_j^2 \left( C_{\mathbf{IP}} \left( \frac{s}{s_0} \right)^{\alpha_{\mathbf{IP}}(t)-1} F(t) \right. \\ & + C_{\mathbf{IR}} \left( \frac{s}{s_0} \right)^{\alpha_{\mathbf{IR}}(t)-1} F(t) \Big), \\ & + \Sigma_{i,j} C_i^2 C_j^2 \left( C_{\mathbf{IP}} \left( \frac{s}{s_0} \right)^{\alpha_{\mathbf{IP}}(u)-1} F(u) \right. \\ & + C_{\mathbf{IR}} \left( \frac{s}{s_0} \right)^{\alpha_{\mathbf{IR}}(u)-1} F(u) \Big). \end{aligned} \quad (2.2)$$

In the simplest version of the model  $i, j = \rho^0, \omega, \phi$  (only light vector mesons are included). The couplings  $C_i, C_j$  describe the  $\gamma \rightarrow V_{i/j}$  transitions that are calculated based on vector meson dilepton width.  $C_{\mathbf{IP}}$  and  $C_{\mathbf{IR}}$  are extracted from the Regge factorization hypothesis (see, e.g., [16,17]).

$$\mathcal{M}_{VDM}^{J/\psi J/\psi} = g_{J/\psi}^2 C_{\mathbf{IP}}^{J/\psi} \left( \frac{s}{s_0} \right)^{\alpha_{\mathbf{IP}}^{J/\psi J/\psi}(t)-1} F_{J/\psi J/\psi \mathbf{IP}}^H(t) F_{J/\psi J/\psi \mathbf{IP}}^H(t) + g_{J/\psi}^2 C_{\mathbf{IP}}^{J/\psi} \left( \frac{s}{s_0} \right)^{\alpha_{\mathbf{IP}}^{J/\psi J/\psi}(u)-1} F_{J/\psi J/\psi \mathbf{IP}}^H(u) F_{J/\psi J/\psi \mathbf{IP}}^H(u). \quad (2.4)$$

In this case (double  $J/\psi$  fluctuations) only pomeron can be exchanged (no subleading reggeons are possible due to the  $c\bar{c}$  structure of  $J/\psi$  mesons). In this case, for simplicity, we take the simplified trajectories as

$$\alpha_{\mathbf{IP}}^{J/\psi J/\psi}(t) = \alpha_{\mathbf{IP}}^{J/\psi J/\psi}(u) = \alpha_{\mathbf{IP}}^{J/\psi J/\psi}(0). \quad (2.5)$$

Here the  $t/u$  dependencies of the trajectories are totally ignored. In numerical calculations we take  $\alpha_{\mathbf{IP}}^{J/\psi J/\psi}(0) = 1.3-1.4$  (typical hard pomeron). Since the  $J/\psi$  mesons are far off mass shell and more compact than light vector mesons also the form factors must be modified. Here we take them in the form:

$$F_{J/\psi J/\psi \mathbf{IP}}^H(t) = \exp\left(\frac{t - m_{J/\psi}^2}{\Lambda_{J/\psi}^2}\right), \quad (2.6)$$

$$F_{J/\psi J/\psi \mathbf{IP}}^H(u) = \exp\left(\frac{u - m_{J/\psi}^2}{\Lambda_{J/\psi}^2}\right). \quad (2.7)$$

Please note that the form factors are normalized to 1 on the meson ( $J/\psi$ ) mass shell. One could also use monopole-like form factors. These form factors drastically reduce the  $J/\psi J/\psi$  component of the amplitude in comparison to light vector meson components. However, due to compactness of  $J/\psi$  we expect  $\Lambda_{J/\psi}$  to be large. In the calculations

It was shown in [8] that the component is concentrated mainly at small photon transverse momenta which at not too small subsystem energies corresponds to  $z \approx \pm 1$ . The Regge trajectories are usually written in a linear form:

$$\begin{aligned} \alpha_{\mathbf{IP}}(t/u) &= \alpha_{\mathbf{IP}}(0) + \alpha'_{\mathbf{IP}} t/u, \\ \alpha_{\mathbf{IR}}(t/u) &= \alpha_{\mathbf{IR}}(0) + \alpha'_{\mathbf{IR}} t/u. \end{aligned} \quad (2.3)$$

These linear forms are valid at not too large  $|t|$  or  $|u|$ . At large  $|t|$  or  $|u|$  the energy dependent factors are artificially small. Therefore here where we explore it more, we propose to smoothly switch off the  $t/u$  dependent terms in (2.3) at  $t \sim -0.5 \text{ GeV}^2$  and  $u \sim -0.5 \text{ GeV}^2$ . The actual place where it should be done is not known precisely. Another option would be to use  $\sqrt{t/u}$  trajectories [18,19].

We also wish to analyze whether more heavy vector mesons such as  $J/\psi$  can give a sizeable contribution.

For example, for the double  $J/\psi$  fluctuations (both photons fluctuate into virtual  $J/\psi$  mesons) we take the following ansatz for the helicity conserving amplitude:

presented here, we take  $\Lambda_{J/\psi} = 2 \text{ GeV}$  for illustration. The actual number is not well known. Also, the normalization parameter  $C_{\mathbf{IP}}^{J/\psi}$  is not well known. It is expected to be smaller than for light vector mesons.

In a similar fashion, one could include one  $J/\psi$  fluctuation and one light vector meson fluctuation. However, there the choice of trajectories is unclear. We will leave these components for future detailed studies.

Finally, let us discuss the helicity structure of the double photon hadronic fluctuation amplitude. We write

$$\mathcal{M}_{\lambda_1 \lambda_2 \rightarrow \lambda_3 \lambda_4}^{(t)} = A(t) \delta_{\lambda_1 \lambda_3} \delta_{\lambda_2 \lambda_4}, \quad (2.8)$$

$$\mathcal{M}_{\lambda_1 \lambda_2 \rightarrow \lambda_3 \lambda_4}^{(u)} = A(u) \delta_{\lambda_1 \lambda_4} \delta_{\lambda_2 \lambda_3}. \quad (2.9)$$

$A(t)$  and  $A(u)$  are given explicitly in (2.2). Then the total double VDM amplitude, including  $t$  and  $u$  processes, reads

$$\mathcal{M}_{\lambda_1 \lambda_2 \rightarrow \lambda_3 \lambda_4}^{VDM} = \frac{1}{\sqrt{2}} \left( \mathcal{M}_{\lambda_1 \lambda_2 \rightarrow \lambda_3 \lambda_4}^{VDM,(t)} + \mathcal{M}_{\lambda_1 \lambda_2 \rightarrow \lambda_3 \lambda_4}^{VDM,(u)} \right). \quad (2.10)$$

Having the double VDM helicity amplitudes, we can add different mechanisms coherently:

$$\mathcal{M}_{\lambda_1 \lambda_2 \rightarrow \lambda_3 \lambda_4} = \mathcal{M}_{\lambda_1 \lambda_2 \rightarrow \lambda_3 \lambda_4}^{\text{boxes}} + \mathcal{M}_{\lambda_1 \lambda_2 \rightarrow \lambda_3 \lambda_4}^{VDM} + \mathcal{M}_{\lambda_1 \lambda_2 \rightarrow \lambda_3 \lambda_4}^{\pi^0} + \dots \quad (2.11)$$

In the following, we shall discuss the sum of the larger two components (boxes and VDM) and quantify their interference effects.

### C. Nuclear cross section

In the present paper, the nuclear cross section is calculated using an equivalent photon approximation in the  $b$  space. In this approach, the diphoton cross section can be written as (see [20])

$$\begin{aligned} & \frac{d\sigma(PbPb \rightarrow PbPb\gamma\gamma)}{dy_{\gamma_1} dy_{\gamma_2} dp_{t,\gamma}} \\ &= \int \frac{d\sigma_{\gamma\gamma \rightarrow \gamma\gamma}(W_{\gamma\gamma})}{dz} N(\omega_1, b_1) N(\omega_2, b_2) S_{\text{abs}}^2(b) \\ & \times d^2b d\bar{b}_x d\bar{b}_y \frac{W_{\gamma\gamma}}{2} \frac{dW_{\gamma\gamma} dY_{\gamma\gamma}}{dy_{\gamma_1} dy_{\gamma_2} dp_{t,\gamma}} dz, \end{aligned} \quad (2.12)$$

where  $\bar{b}_x = (b_{1x} + b_{2x})/2$  and  $\bar{b}_y = (b_{1y} + b_{2y})/2$ . The relation between  $\vec{b}_1, \vec{b}_2$  and impact parameter:  $b = |\vec{b}| = \sqrt{|\vec{b}_1|^2 + |\vec{b}_2|^2 - 2|\vec{b}_1||\vec{b}_2| \cos \phi}$ . Absorption factor  $S_{\text{abs}}^2(b)$  is calculated as

$$S_{\text{abs}}^2(b) = \Theta(b - b_{\text{max}}) \quad (2.13)$$

or

$$S_{\text{abs}}^2(b) = \exp(-\sigma_{NN} T_{AA}(b)), \quad (2.14)$$

where  $\sigma_{NN}$  is the nucleon-nucleon interaction cross section, and  $T_{AA}(b)$  is related to the so-called nuclear thickness,  $T_A(b)$ ,

$$T_{AA}(|\vec{b}|) = \int d^2\rho T_A(\vec{\rho} - \vec{b}) T_A(\rho), \quad (2.15)$$

and the nuclear thickness is obtained by integrating the nuclear density

$$T_A(\vec{\rho}) = \int \rho_A(\vec{r}) dz, \quad \vec{r} = (\vec{\rho}, z), \quad (2.16)$$

where  $\rho_A$  is the nuclear charge distribution. The nuclear photon fluxes  $N(\omega_1, b_1)$  and  $N(\omega_2, b_2)$  are calculated with realistic charge distribution, as described in [21].

So far, in our previous works, we presented UPC results only with a sharp cut on the impact parameter, which reflects the distance between two nuclei with a value equal to exactly two radii of the nuclei, i.e.,  $b > 14$  fm for Pb + Pb collisions. Due to the no homogeneous nuclear charge distribution, it seems to be more reasonable to use the absorption factor given by Eq. (2.14).

### D. Background contribution

It was discussed in [7] that the  $\gamma\gamma \rightarrow \pi^0(\rightarrow 2\gamma)\pi^0(\rightarrow 2\gamma)$  reaction constitutes a difficult background for the  $\gamma\gamma \rightarrow \gamma\gamma$  measurements at intermediate  $M_{\gamma\gamma}$ . How to calculate the cross section for  $\gamma\gamma \rightarrow \pi^0\pi^0$  reaction was discussed in [22] and will not be repeated here. The calculation of the background proceeds in three steps. First, the cross section for  $\gamma\gamma \rightarrow \pi^0\pi^0$  is calculated (for details, see [22]). Next the cross section for  $AA \rightarrow AA\pi^0\pi^0$  is computed in the equivalent photon approximation in an analogous way as described in the previous subsection. Finally, the simulation of both  $\pi^0$  decays is performed and combined distributions of one photon from the first  $\pi^0$  and one photon from the second  $\pi^0$  are constructed.

## III. RESULTS: ELEMENTARY CROSS SECTION

Treating photons as massless particles, one can expect the absence of a minimum energy value, which is determined by the kinematical threshold. In Fig. 2 we show the dependence of the elementary cross section on energy in the  $\gamma\gamma$  system. Fig. 2(a) demonstrates that putting a cut on the energy of the two-photon system (the red dashed vertical line indicates the value of  $W_{\gamma\gamma} = 5$  GeV), we automatically get rid of a significant signal contribution. The pointed limitation is due to the existing restriction of the detectors measuring light-by-light scattering in the ATLAS and CMS experiments. Focusing on the details of box contribution, Fig. 2(b), we show individual contributions of different boxes (electron, muon, quarks). In Fig. 2(c) we show the relative effect of including different loops. This figure nicely demonstrates the role of quarkish loops. They change the cross section by 40–50% depending on the  $\gamma\gamma$  energy. This is a large extent due to interference of quarkish and leptonic loops. Without the interference, the effect is about 10% (see the short dashed line). One can see that at low diphoton invariant masses, the electronic loops dominate. The quarkish loops become sizeable only at  $W_{\gamma\gamma} > 1$  GeV. At an energy of  $W_{\gamma\gamma} > 2m_\tau$  one can observe a slight enhancement of the fermionic contribution, which illustrates the presence of  $\tau$  leptons in the loop.

In Fig. 3 we show  $d\sigma/dz$  for  $\gamma\gamma \rightarrow \gamma\gamma$  for (a) boxes, (b) double hadronic fluctuation calculated within the VDM-Regge approach, and (c) the  $\pi^0$  exchange [Fig. 1(e)] calculated as in Ref. [15]. Results are presented for five fixed values of energy in the range of (1 – 50) GeV. At larger energies, the VDM-Regge contribution peaks at  $z = \pm 1$ . On the other hand, the  $\pi^0$  exchange contribution has minima at  $z = \pm 1$  which is due to the structure of corresponding vertices. The latter contribution is relatively small. In general, the box contributions dominate, especially for low photon-photon scattering energies. At larger scattering energies ( $W_{\gamma\gamma} > 2$  GeV) the VDM-Regge contribution competes with the box contributions

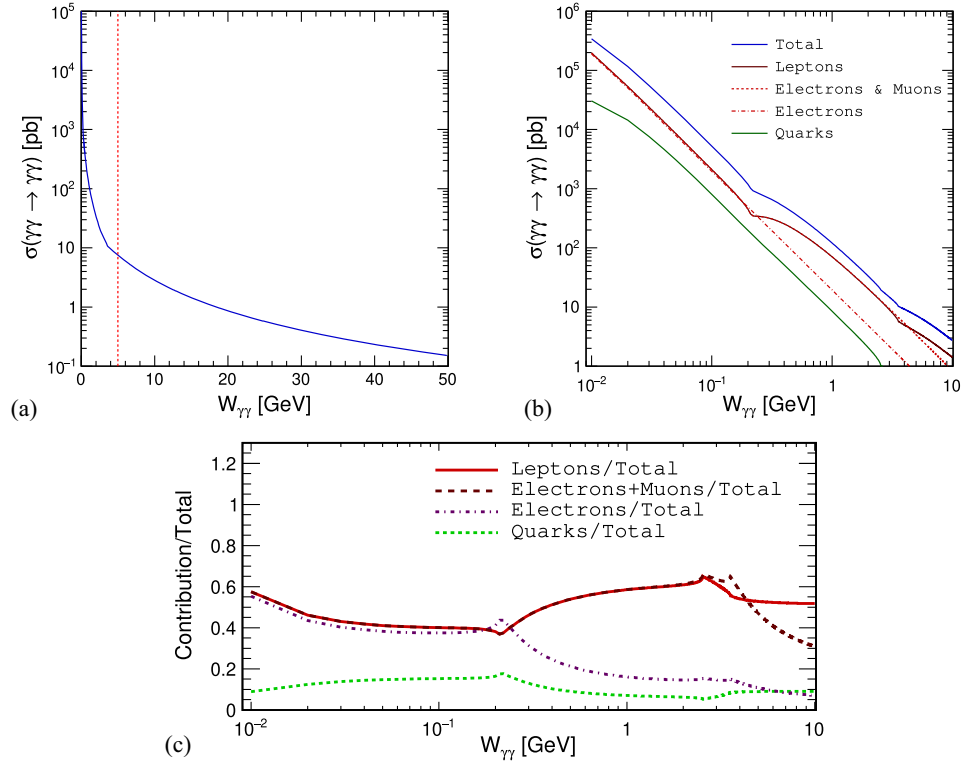


FIG. 2. Elementary cross section (in pb) as a function of energy. Results for fermionic boxes are shown over a wide range of energies: (a) linear scale and focusing on the MeV range and (b) where the logarithmic scale is used. The total cross section (blue solid line) is split somewhat artificially into quarks (green solid line), electrons (red dashed line), electrons and muons (red dotted line), and leptons (red solid line) contributions; (c) shows a ratio of each contribution to a coherent sum of them. The red solid line represents leptonic cross section divided by total cross section, the green dotted line refers to quarks, magenta dash-dotted line to electrons and dashed dark-red line applies to a sum of electron and muon contributions.

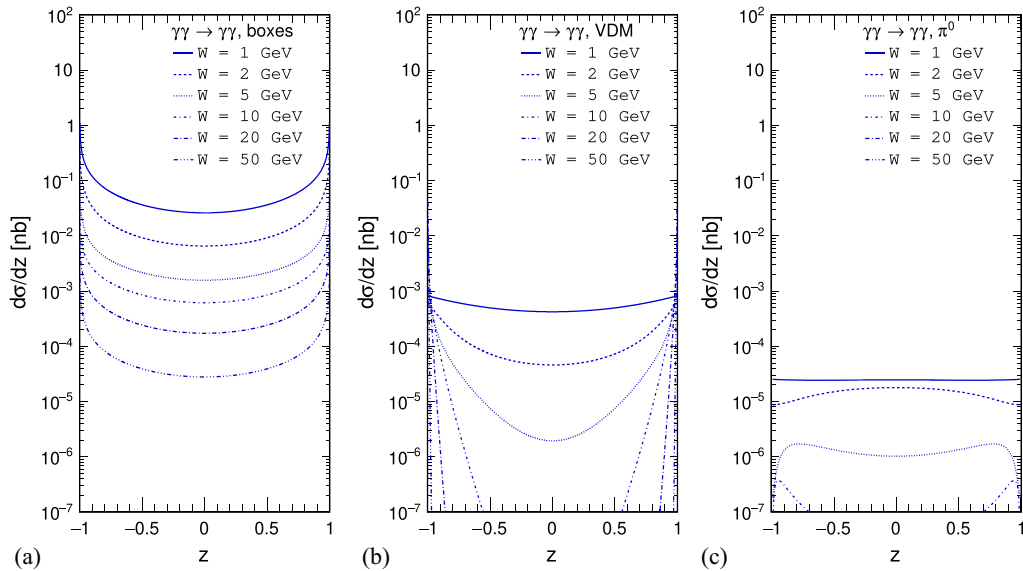


FIG. 3.  $\cos(\theta)$  distributions for (a) boxes, (b) double hadronic fluctuations, and (c)  $\pi^0$  exchange for different energies  $W = 1, 2, 5, 10, 20, 50$  GeV.

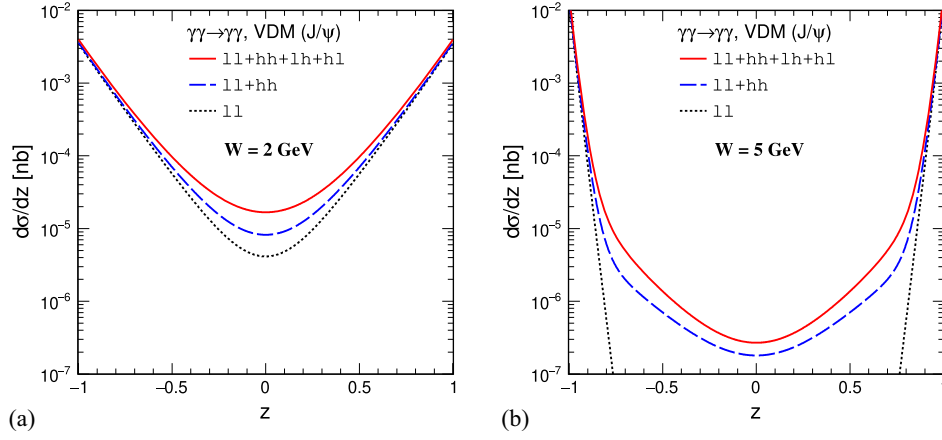


FIG. 4. Modification of  $d\sigma/dz$  due to including fluctuations with virtual  $J/\psi$  mesons: (a)  $W = 2$  GeV, (b)  $W = 5$  GeV. The top solid line includes all components [light ( $l$ ) and heavy ( $h$ ) vector mesons], the dotted line only light vector mesons.

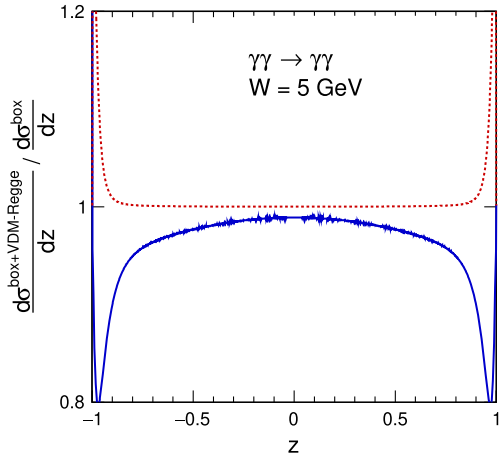


FIG. 5. The ratio of the coherent (blue) and incoherent (red) sum of the box and VDM-Regge contributions divided by the cross section for the box contribution alone for  $W = 5$  GeV.

only at  $z \sim \pm 1$ . Can one expect, in this context, sizeable interference effects of both mechanisms?

Now we wish to concentrate briefly on the second biggest in Fig. 3 contribution, double photon fluctuations. We include both light vector mesons  $\rho^0$ ,  $\omega$ ,  $\phi$  as well as  $J/\psi$  (one or two) as described in the theoretical section. Our results, for two collision energies ( $W = 2, 5$  GeV), are shown in Fig. 4. The dotted line includes only light vector meson fluctuations, the dashed line in addition double  $J/\psi$  fluctuations and the solid line all combinations of photon fluctuations. The inclusion of  $J/\psi$  meson fluctuations leads to an enhancement of the cross section at  $-0.5 < z < 0.5$ . The enhancement is more spectacular for larger collision energy. The corresponding cross section there is, however, much smaller than the box contribution (see Fig. 3).

Fig. 5 determines the quantitative changes in the box results after adding the VDM-Regge contribution. In Fig. 5

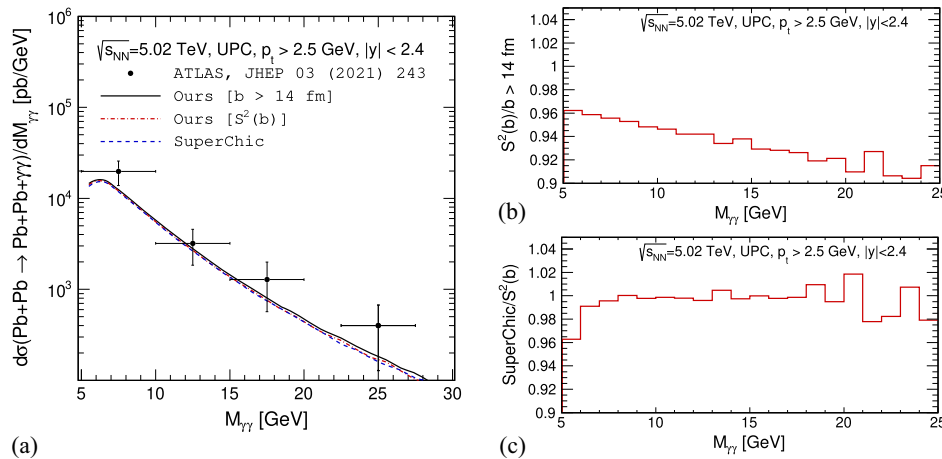


FIG. 6. Differential cross section as a function of two-photon invariant mass at  $\sqrt{s_{NN}} = 5.02$  TeV. (a) The ATLAS experimental data are collected with theoretical results including a sharp cut on impact parameter ( $b > 14$  fm, solid black line) and smooth nuclear absorption factor  $S^2(b)$  (dash-dotted red line). For completeness, results that are obtained with the help of Eq. (2.12) are compared with results from SuperChic [23]. The right panel shows two ratios: (b) distributions calculated within our approach with sharp and smooth cutoff on impact parameter and (c) SuperChic result to our result, using a smooth representation of the gap survival factor.

TABLE I. Total cross section for  $\text{PbPb} \rightarrow \text{PbPb}\gamma\gamma$  in nb obtained in different approaches for experimental ATLAS/CMS kinematics: collision energy  $\sqrt{s_{NN}} = 5.02$  TeV, diphoton invariant mass  $M_{\gamma\gamma} > 5$  GeV, photon rapidity  $|y| < 2.4$ . ATLAS and CMS detected photons in different range of transverse momenta.

Experiment	$p_{t,\min}$ [GeV]	UPC condition	$\sigma_{\text{tot}}$ [nb]
ATLAS	2.5	$b > 14$ fm	$81.062 \pm 0.05$
		$S^2(b)$ Eq. (2.14)	$77.084 \pm 0.005$
		SuperChick	$76.421 \pm 0.074$
CMS	2	$b > 14$ fm	$105.986 \pm 0.067$
		$S^2(b)$ Eq. (2.14)	$102.104 \pm 0.057$
		SuperChick	$100.101 \pm 0.144$

we show the ratio of cross sections when including the VDM-Regge contribution to that for box contribution. In this calculation, only the VDM-Regge component's active helicity contributions (six combinations) are included. The red line represents the incoherent sum, while the blue line also includes interference effects. In this calculation, the so-called sqrt trajectories [18,19] were used. We observe a negative interference effect. Adding the remaining contributions would lead to additional deviations.

#### IV. RESULTS: NUCLEAR CROSS SECTION

Now we go to nuclear UPC and will show our results for four experimental kinematic conditions, each in a separate subsection.

##### A. ATLAS and CMS kinematics

We start by confronting our calculations with the current ATLAS data [5]. Figure 6(a) shows diphoton invariant mass distribution [5]. This result slightly depends on the treatment of absorption corrections in the  $b$  space. The results of the two different approximations (as described in the figure

caption) almost coincide. For comparison, we show results obtained with the SuperChic generator [23]. We get a reasonable agreement taking into account relatively large error bars of experimental data (small statistics). Right panel of Fig. 6 presents the ratio of nuclear results from our approach [Eq. (2.12)] comparing smooth cutoff [Eq. (2.14)] and sharp cutoff on impact parameter ( $b > 14$  fm) corresponds to results from SuperChic generator [23]. The difference between results obtained with smooth and sharp cut in ultraperipheral condition becomes larger with larger value of diphoton invariant mass, Fig. 6(b). However, applying the same type of condition to the impact parameter, i.e., comparing the results from the SuperChic generator and that of our calculation, gives a difference of about 2%. A similar conclusion arises after comparing the total cross sections listed in Table I. Taking into account the possibility of different initial UPC conditions, the used methods describe the experimental data of ATLAS [3,5,6] and CMS [4] in a similar way.

In Fig. 7 we show results with a sharp cutoff,  $b > 14$  fm, and when including the smooth dependence of  $S_{\text{abs}}^2(b)$  on impact parameter. In Fig. 7(a), we show somewhat academic impact parameter distribution (not measurable) while in Fig. 7(b), rapidity distribution of outgoing system,  $Y_{\gamma\gamma} = (y_1 + y_2)/2$ . Only small differences due to the treatment in the  $b$  space [about (3–4)%] at midrapidities can be observed.

Having described the ATLAS data, we wish to discuss new unexplored kinematics regions.

##### B. Broad range of rapidity, full phase space

Now we go to the somewhat broader range of rapidity and allow for very small transverse momenta. In Fig. 8 we show two-dimensional distribution in  $(M_{\gamma\gamma}, p_{t,\gamma})$ . We observe a strong enhancement for  $M_{\gamma\gamma} \approx 2p_t$ , which infers that small  $p_{t,\gamma}$  means automatically small  $M_{\gamma\gamma}$  and vice versa.

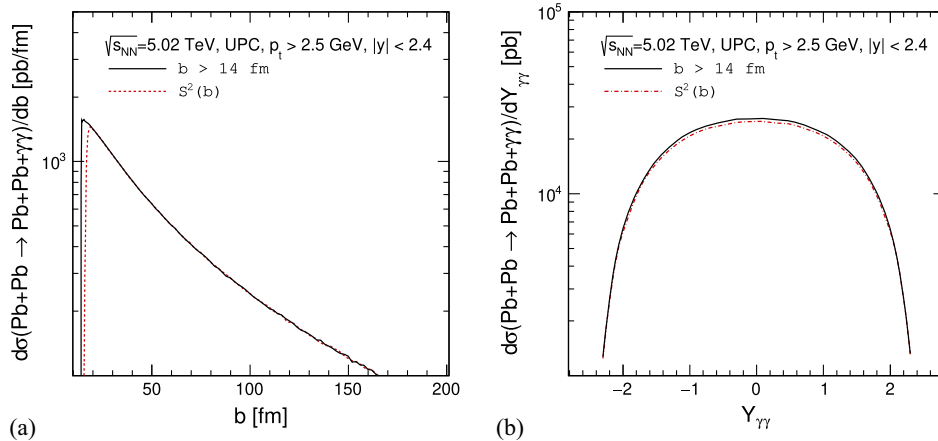


FIG. 7. (a) Impact parameter and (b) rapidity distribution for UPC of lead-lead at collision energy  $\sqrt{s_{NN}} = 5.02$  TeV. The solid line corresponds to a sharp cut on the impact parameter and the red dash-dotted line is for the absorption factor as given by Eq. (2.14).

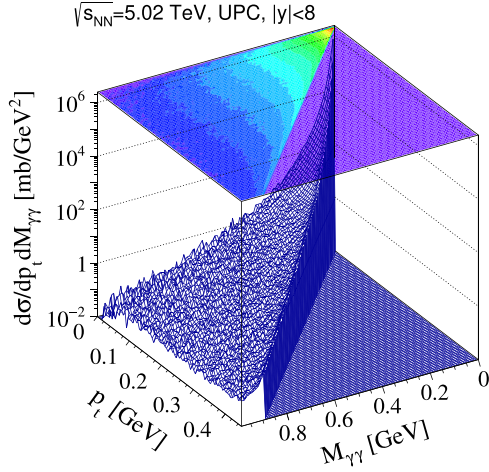


FIG. 8. Two-dimensional distribution in photon transverse momentum and diphoton invariant mass for UPC of lead-lead collisions in a wide photon rapidity range  $y \in (-8, 8)$ , starting from  $p_t > 5$  MeV.

TABLE II. Total cross section in mb for  $\text{PbPb} \rightarrow \text{PbPb}\gamma\gamma$  for different fermionic contributions artificially separated. Here collision energy  $\sqrt{s_{NN}} = 5.02$  TeV, diphoton invariant mass  $M_{\gamma\gamma} = (0.01 - 1)$  GeV, photon transverse momentum  $p_t > 5$  MeV and photon rapidity  $|y| < 8$ .

	$\sigma_{\text{tot}}$ [mb]
Total	$91.675 \pm 0.023$
Electrons + Muons	$41.597 \pm 0.010$
Electrons	$39.163 \pm 0.010$
Quarks	$12.483 \pm 0.003$

In Fig. 9 we show different distributions in (a)  $M_{\gamma\gamma}$ , (b)  $p_t$ , and in (c)  $y_\gamma$ . In this figure we present decomposition into different loop contributions (leptons, quarks). The electron/positron loops dominate at low  $M_{\gamma\gamma}$  and low  $p_t$ . Despite the noticeable difference between leptonic and quarkonic contributions, their coherent sum contributes much more than the leptonic contribution alone. Looking at the total cross section values in Table II, although the

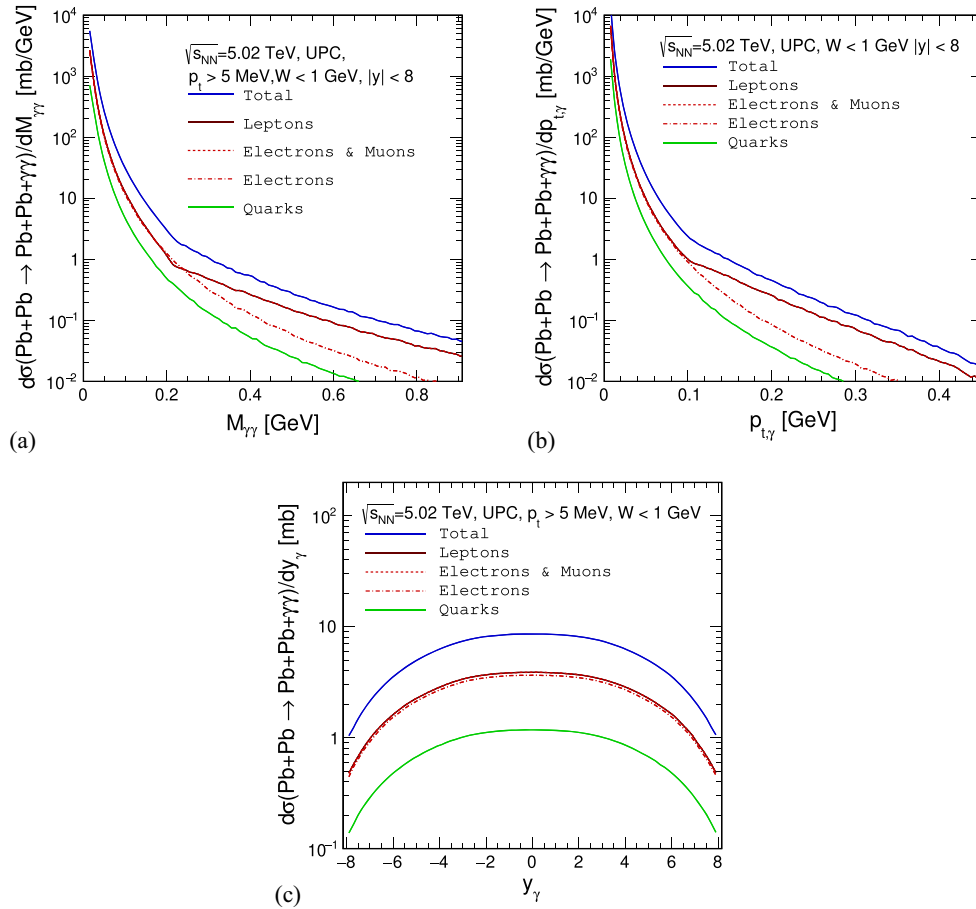


FIG. 9. (a) Diphoton invariant mass, (b) photon transverse momentum, and (c) rapidity distribution in mb for different fermionic contributions in ultraperipheral lead-lead collisions at energy  $\sqrt{s_{NN}} = 5.02$  TeV. The blue solid line corresponds to a sum of all contributions, the red solid line is a sum for leptons, the dashed red line relates to electrons, and the green solid line represents a contribution of quark loops.

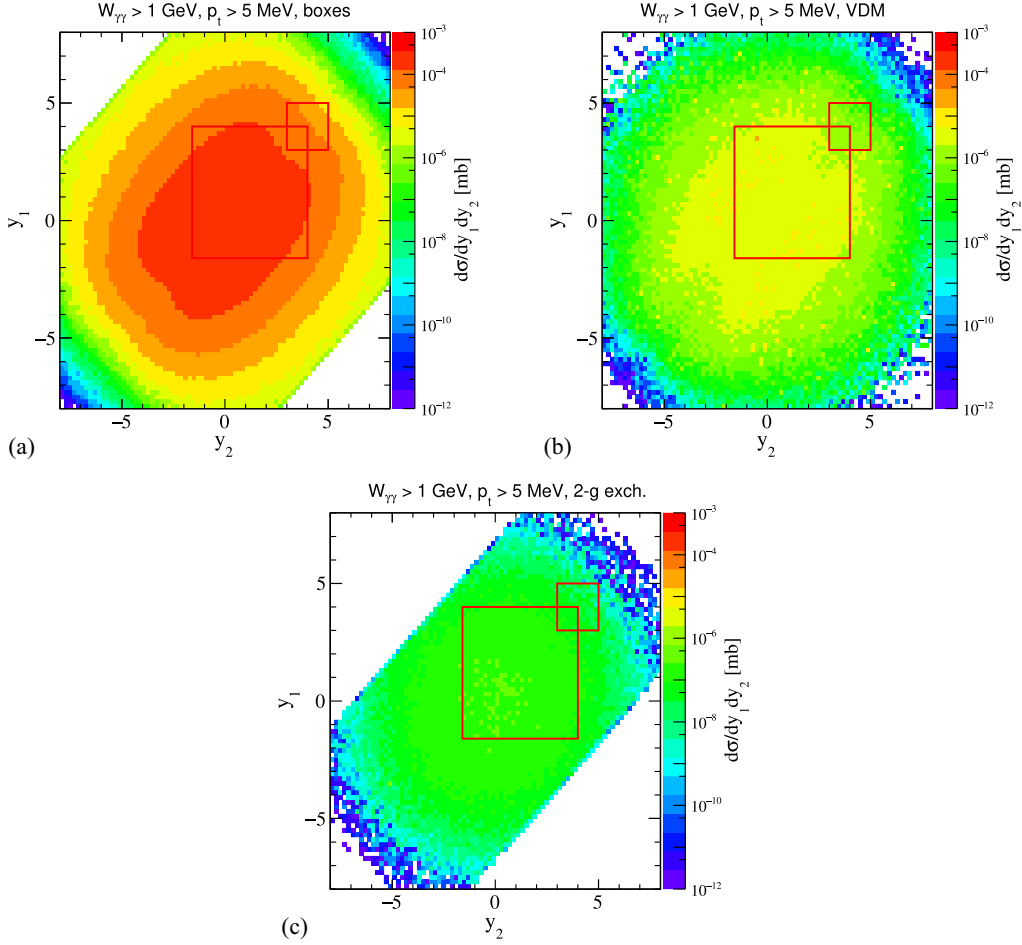


FIG. 10. Distribution in  $(y_1, y_2)$  in mb for photon transverse momentum  $p_t > 5$  MeV, diphoton invariant mass  $M_{\gamma\gamma} > 1$  GeV. (a) Boxes, (b) VDM-Regge mechanism, and (c) two-gluon exchange.

quark contribution is more than twice as small as the lepton contribution ( $\sigma_{\text{tot}}^{\text{quarks}} \approx 30\% \sigma_{\text{tot}}^{\text{leptons}}$ ), summing over the helicities for leptonic and quarkish boxes, yields a result that is more than twice bigger than the lepton contribution ( $\sigma_{\text{tot}}^{\text{leptons}} \approx 45\% \sigma_{\text{tot}}^{\text{fermions}}$ ). These cross sections are calculated for the diphoton invariant mass range up to 1 GeV.

In Figs. 10 and 11 we show corresponding two-dimensional distributions  $(y_1, y_2)$  for three different mechanisms separately: boxes, double-hadronic fluctuations and two-gluon exchange. In this inclusive case (integration over  $p_t = p_{1t} = p_{2t}$  and  $W_{\gamma\gamma}$ ) we observe that VDM-Regge and two-gluon mechanisms give much smaller contribution than the box mechanisms, at least at midrapidity. It is slightly different in asymmetric configurations (one photon forward, one photon backward). The red contours represent the rapidity limit for ALICE 3:  $-1.6 < y_\gamma < 4$  and  $3 < y_\gamma < 5$ . The largest cross section occurs in the midrapidity of both photons. Within this rapidity range, it is expected to be able to detect photons with  $p_{t,\gamma} > 100$  MeV. Our predictions show that in the forward range of the calorimeter,  $3 < y_\gamma < 5$ , even though the VDM-Regge contribution is about three orders of magnitude smaller

than fermionic boxes, it should be included to determine the coherent sum of these two processes.

In Fig. 12 we present diphoton invariant mass distributions for different mechanisms including (a)  $\pi^0$ ,  $\eta$ , and  $\eta'$  resonances [Fig. 1(d)]<sup>1</sup> as well as (b) VDM-Regge and two-gluon exchange mechanisms. While the resonances stick over the box continuum they can be easily eliminated imposing windows around the resonance positions. Although, at first glance, the contribution from higher order mechanisms seems insignificant, it is important to be aware that the VDM-Regge contribution is only an order of magnitude smaller than the leading contribution from the fermionic boxes.

The corresponding distributions in  $p_t = p_{1t} = p_{2t}$  are shown in Fig. 13. We observe huge enhancements of the cross section at  $p_t \sim M_R/2$  (Jacobian peak). It would be interesting to see such enhancements experimentally for controlling the general situation. Imposing the windows around resonances would allow us to eliminate the resonance contributions. However, this would probably distort to some extent other distributions, in particular, those for

<sup>1</sup>In Ref. [24] also  $\eta_c$  resonance was considered.

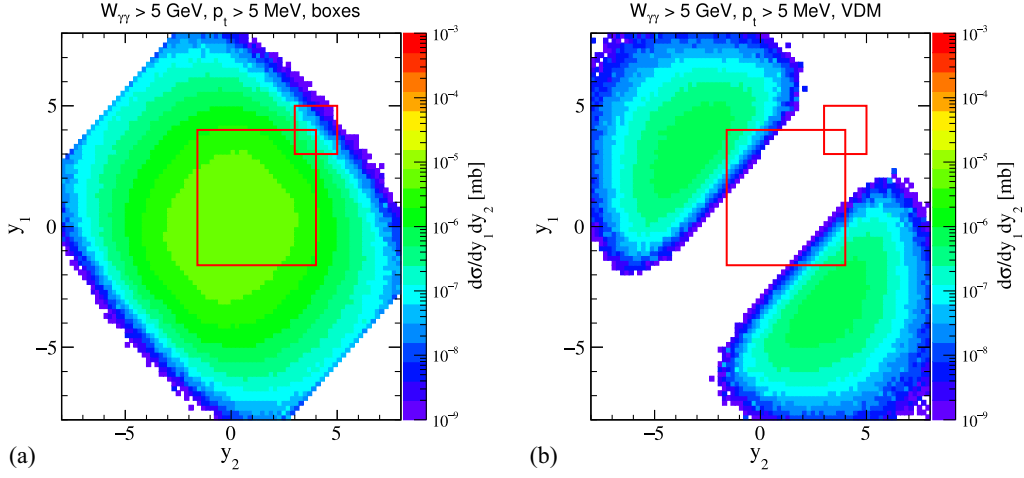


FIG. 11. Distribution in  $(y_1, y_2)$  in mb for transverse momentum  $p_t > 5$  MeV, diphoton invariant mass  $M_{\gamma\gamma} > 5$  GeV. (a) Boxes, (b) VDM-Regge mechanism.

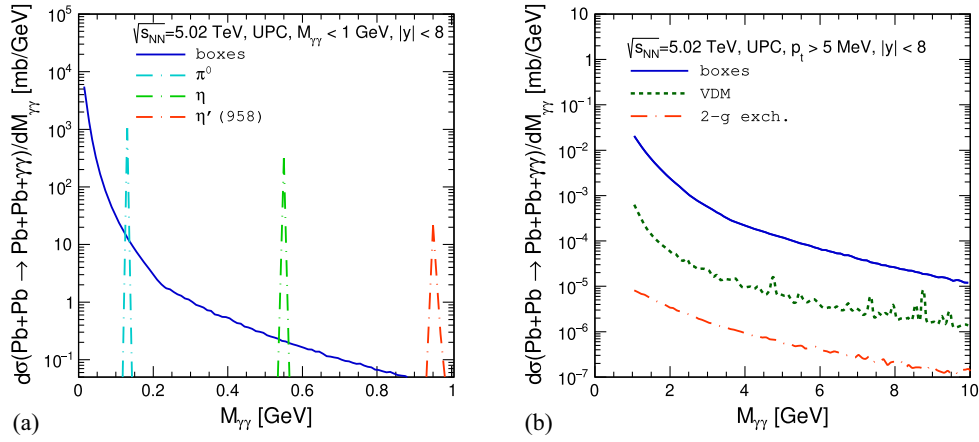


FIG. 12. Diphoton invariant mass distribution for photon transverse momentum  $p_t > 5$  MeV and photon rapidities  $y_{1/2} \in (-8, 8)$ . (a) Boxes vs resonances,  $M_{\gamma\gamma} < 1$  GeV. (b) Boxes vs VDM-Regge and vs two-gluon exchange contribution,  $M_{\gamma\gamma} > 1$  GeV.

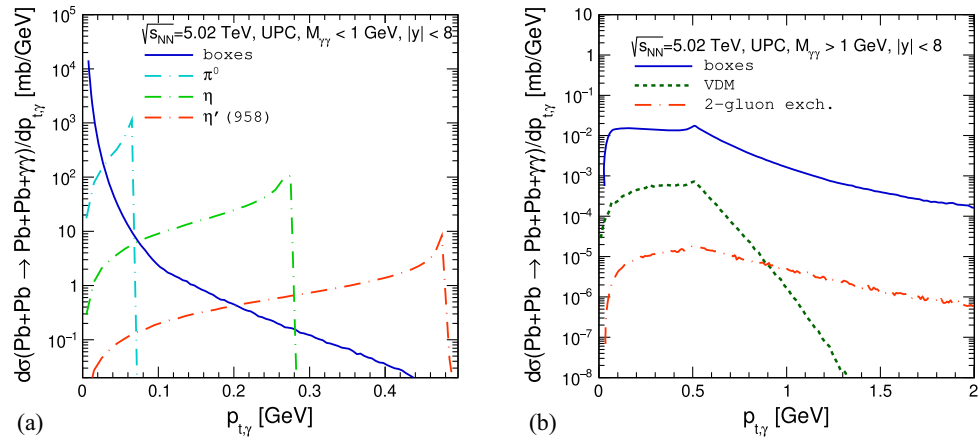


FIG. 13. Transverse momentum distribution for photon transverse momentum  $p_t > 5$  MeV, diphoton invariant mass  $M_{\gamma\gamma} < 1$  GeV and photon rapidities  $y_{1/2} \in (-8, 8)$ . (a) Boxes vs resonances; (b) boxes vs VDM-Regge vs two-gluon exchange.

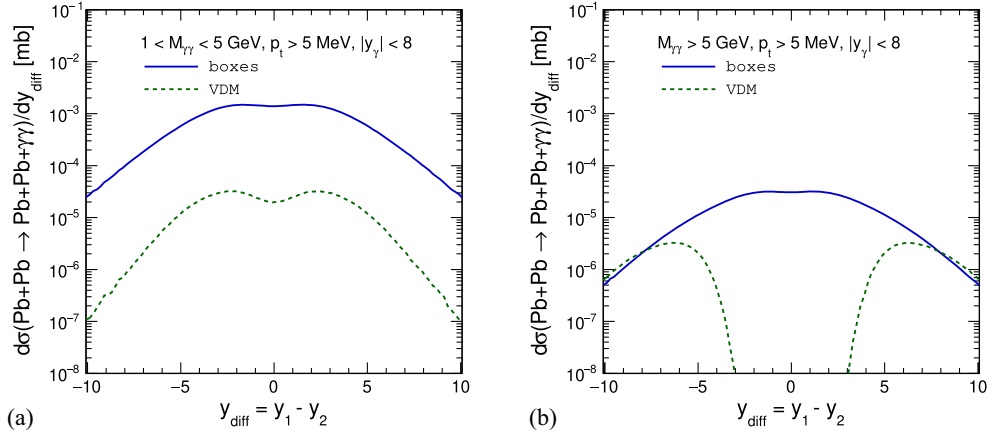


FIG. 14. Distribution in  $y_{\text{diff}}$  for light-by-light scattering processes in  $\text{PbPb} \rightarrow \text{PbPb}\gamma\gamma$ . Here the transverse momentum cut is equal to 5 MeV. The blue solid line relates to the boxes, and the green dotted line to the VDM-Regge contribution. Here the range of measured diphoton invariant mass is (a) (1 – 5) GeV, (b) > 5 GeV.

$p_t = p_{1t} = p_{2t}$ . Therefore it is not clear to us whether such cuts would be welcomed.

For completeness, in Fig. 14 we show distributions in rapidity difference hoping it could distinguish different mechanisms. Indeed the shape of the distributions corresponding to two-photon hadronic fluctuations seems somewhat broader than that for boxes. There is a region of  $y_{\text{diff}}$  where the VDM-Regge contribution is as big as that for fermionic boxes. This region of phase space is, however, not easy to measure at the LHC. The resonance contributions, not shown here explicitly, are concentrated at  $-2 < y_{\text{diff}} < 2$  but for  $M_{\gamma\gamma} > 5$  GeV the light mesons are automatically removed. We shall discuss the resonance contribution for ALICE 3.

### C. ALICE and FoCal

The FoCal detector planned for run 4 was described in [13]. It is a general purpose detector. It can also measure photons.

We start our presentation from the results when in addition both photons are measured by FoCal. In Fig. 15(a) we show results when both photons have energies bigger than 200 MeV. In addition, we show the  $\pi^0\pi^0$  background. In this case, only two photons are measured. Without additional cuts, the background is clearly bigger than the signal. However, by imposing extra conditions on vector asymmetry, we can lower the background contribution. The vector asymmetry defined in Ref. [7] as

$$A_V = |\vec{p}_{t,1} - \vec{p}_{t,2}| / |\vec{p}_{t,1} + \vec{p}_{t,2}|, \quad (4.1)$$

reflects a convolution of each photon transverse momentum vector.

At very low  $M_{\gamma\gamma}$  the  $\pi^0\pi^0$  background is negligible, which opens a new window to measure the  $\gamma\gamma \rightarrow \gamma\gamma$  scattering at  $M_{\gamma\gamma} < 1$  GeV while for the ATLAS experiment it was  $M_{\gamma\gamma} > 5$  GeV. In Fig. 15(b) we show similar

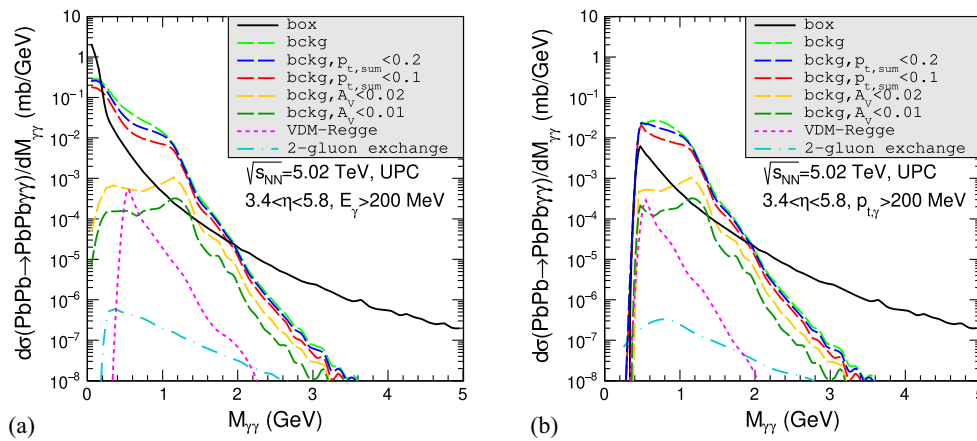


FIG. 15. Invariant mass distribution for the nuclear process. Predictions are made for the future FoCal acceptance, i.e., (a)  $E_{1,\gamma} > 200$  MeV and  $3.4 < y_{\gamma/2} < 5.8$ , (b)  $p_{t,\gamma} > 200$  MeV and  $3.4 < y_{\gamma/2} < 5.8$ . Here, both photons are “measured” in FoCal. The background contribution is presented for different elimination cuts.

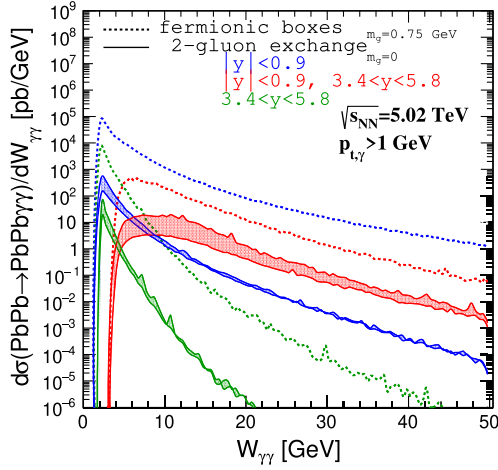


FIG. 16. Diphoton invariant mass distribution for  $\text{PbPb} \rightarrow \text{PbPb}\gamma\gamma$  process for ALICE, FoCal, and their combination.

results when imposing  $p_{t,\gamma}$  condition. In this case, it is rather difficult to eliminate the  $\pi^0\pi^0$  background. Here the VDM-Regge component is relatively small. In Fig. 5 we have shown that at  $W_{\gamma\gamma} \approx 5$  GeV some effect of the VDM-Regge component could potentially be observed. However,

the cuts on transverse momenta remove this part of the phase space. Comparing the results for the same cut on the energy of each outgoing photon, Fig. 15(a), and on the transverse momentum of the photon, Fig. 15(b), one can observe that the limit on  $p_{t,\gamma}$  removes a very large contribution to the total cross section, which is located in a small diphoton invariant mass.

Another option is to use simultaneously the FoCal and the main ALICE detector. In Fig. 16, we simultaneously show the box and two-gluon exchange contributions. In this calculation, we assumed that the transverse momenta of both photons have  $p_t > 1$  GeV. In this case, the separated two-gluon exchange contribution is only an order of magnitude smaller than the box contribution. The shaded band is due to an “unknown” effective gluon mass.

In Fig. 17 we show similar distributions but for  $p_t > 0.2$  GeV and combined ALICE and FoCal rapidity region. Here in some regions of the phase space, the VDM-Regge contribution could be seen as a 10% modification of the cross section with respect to the calculations with only boxes. Here the separated VDM-Regge component is even bigger. We conclude that already at run 4 one could indirectly observe a signature of other mechanisms than

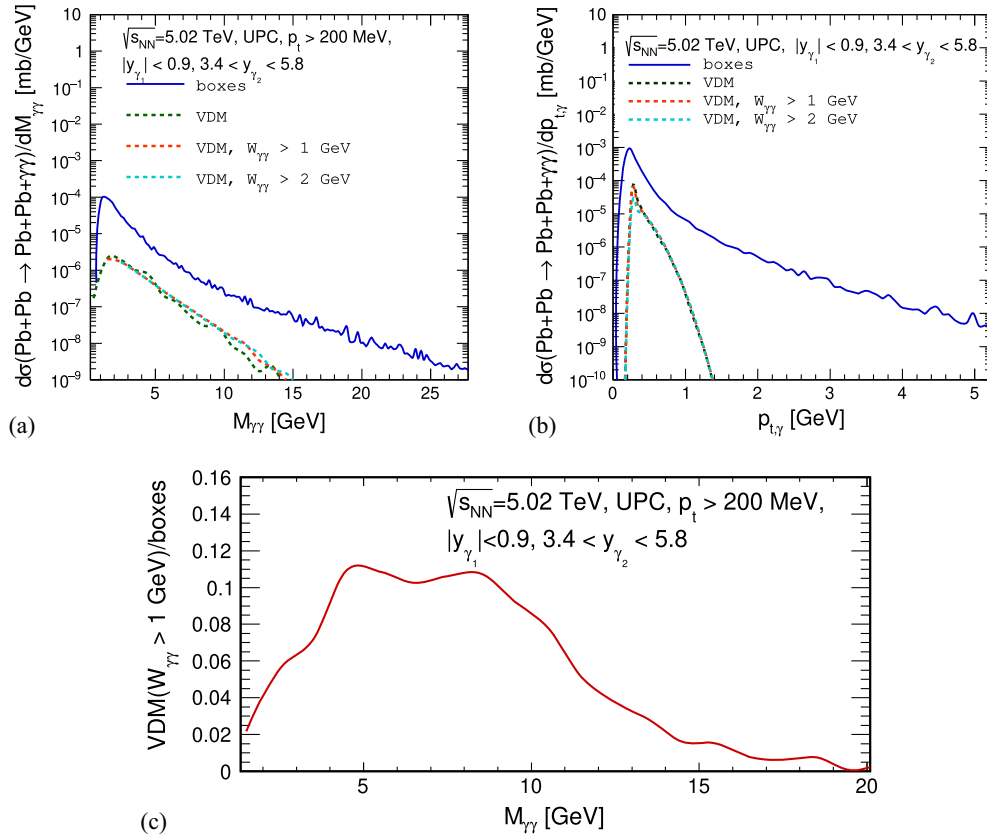


FIG. 17. Prediction for the FoCal detector in association with midrapidity ALICE detector for photons:  $p_t > 200$  MeV, diphoton mass  $M_{\gamma\gamma} > 400$  MeV, and photon rapidities  $|y_1| < 0.9$  and  $y_2 \in (3.4, 5.8)$ . The blue line corresponds to fermionic loops and the green lines to the VDM-Regge contribution. (a) Diphoton invariant mass distribution, (b) photon transverse momentum distribution, (c) ratio of the VDM-Regge ( $W_{\gamma\gamma} > 1$  GeV) and box contributions as a function of diphoton invariant mass. No interference effects are included here.

fermionic boxes. In Fig. 17(c) we present the ratio of results from Fig. 17(a). We see that the VDM-Regge contribution reaches about 10% at  $M_{\gamma\gamma} \approx 4\text{--}10$  GeV. Whether the experimental measurement could demonstrate the existence of the VDM-Regge contribution remains an open question due to model uncertainties. However, we predict deviations from the box calculation at relatively well-localized region of diphoton invariant masses  $M_{\gamma\gamma} \approx 4\text{--}10$  GeV.

#### D. ALICE 3 kinematics

Now we wish to show distributions relevant for the ALICE 3 detector.

In Fig. 18 we show distributions in diphoton invariant mass for photons  $-4 < y_1, y_2 < 4$  and  $E_\gamma > 50$  MeV (see Ref. [14]). We show the light-by-light box contribution (solid line) as well as the  $\pi^0\pi^0$  background contribution (red lines). At diphoton invariant masses,  $0.5 \text{ GeV} < M_{\gamma\gamma} < 1$  GeV, the background contribution is almost as big as the signal contribution. As discussed in [7] it can be to some extent reduced. Although the background is smaller than fermionic boxes in the full range of diphoton invariant mass, it can be further reduced by imposing the cut on  $|\vec{p}_{1t} + \vec{p}_{2t}| < 0.1$  GeV and vector asymmetry  $A_V < 0.02$ . Imposing a cut on the background causes that the background in the whole diphoton invariant mass range is much smaller than the signal.

In Fig. 19 we show analogous distribution in  $y_{\text{diff}} = y_1 - y_2$ . Again different contributions are shown separately. The results for the double- $\pi^0$  background contribution are particularly interesting. It has a maximal contribution at  $y_{\text{diff}} = 0$  and drops quickly for larger  $|y_{\text{diff}}|$ . An extra cut on  $y_{\text{diff}}$  could therefore considerably reduce the unwanted

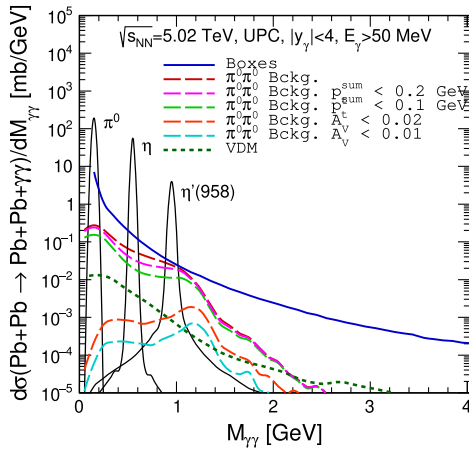


FIG. 18. Diphoton invariant mass distribution for ALICE 3, i.e., rapidity  $y_{1/2} \in (-4, 4)$  and photon energy  $E_\gamma > 50$  MeV. Here the blue solid line relates to the box contribution, the dotted line to the VDM-Regge component and the dashed lines are for double- $\pi^0$  background contribution. Here we impose several extra conditions on diphoton transverse momenta and vector asymmetry.

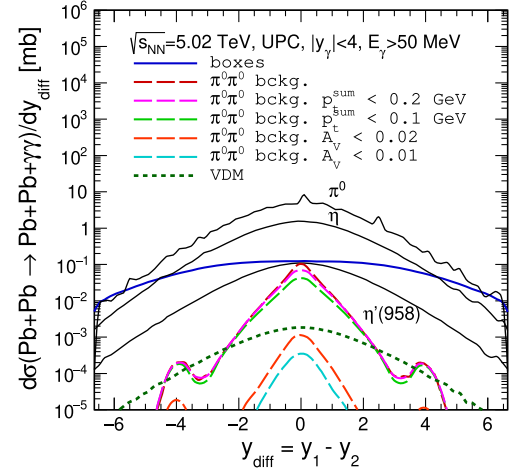


FIG. 19. Differential cross section as a function of  $y_{\text{diff}} = y_1 - y_2$  for extended ALICE 3 kinematics:  $|y_{1/2}| < 4$  and  $E_\gamma > 50$  MeV. Results are presented for boxes, resonances, VDM-Regge mechanisms, and double- $\pi^0$  background.

double- $\pi^0$  contribution. In Fig. 20 we show what happens when we impose the cut on  $y_{\text{diff}}$ . The effect of such a cut on box contribution is relatively small but leads to a huge reduction of the background. The effect of the cut is much larger for small  $M_{\gamma\gamma}$  and therefore should be avoided if one is interested in this region of energies.

In Fig. 21 we show distribution in  $M_{\gamma\gamma}$  (a) and  $p_t$  (b) for a planned special photon detector  $3 < y_\gamma < 5$ . Here  $p_t > 5$  MeV was imposed as described in Ref. [14]. We show that at low  $M_{\gamma\gamma}$  and low  $p_t$  the LbL signal by far exceeds the  $\pi^0\pi^0$  background, even without including any background suppression condition. Here we have assumed  $2\pi$  azimuthal coverage of the special photon detector.

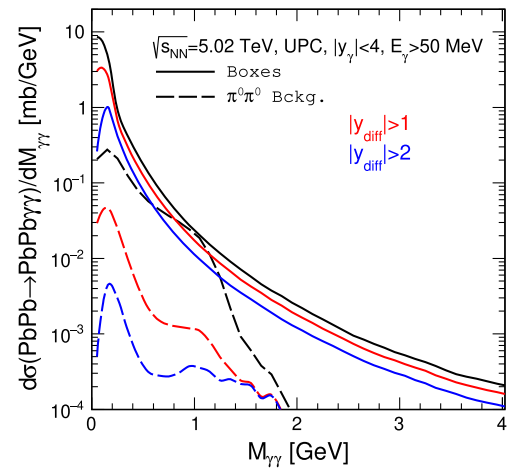


FIG. 20. Influence of extra conditions on  $y_{\text{diff}} = y_1 - y_2$  ( $|y_{\text{diff}}| > 1, 2$ ) on diphoton invariant mass distribution for ALICE 3. Here the solid lines relate to the box contribution and the dashed lines are for the double- $\pi^0$  background.

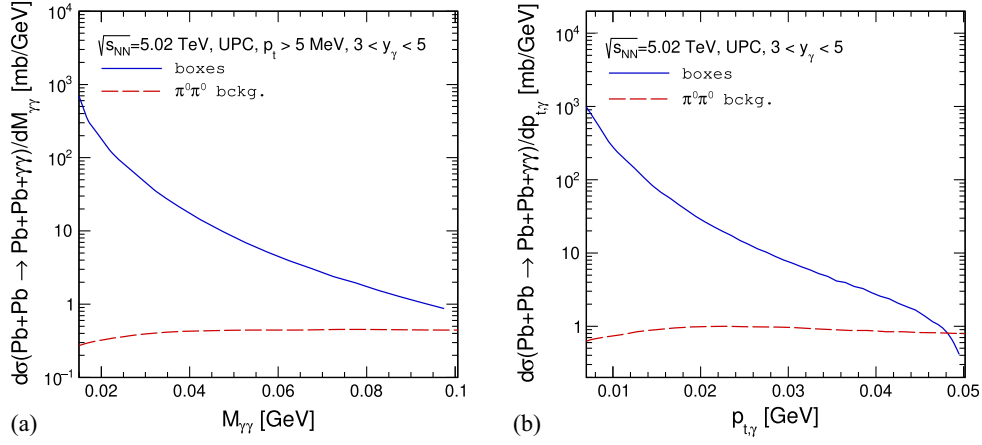


FIG. 21. Prediction for the ALICE 3 experiment for soft photons:  $p_t = (5 - 50)$  MeV and photon rapidities  $y_i \in (3, 5)$ . The blue line corresponds to fermionic loops, the red line relates to the double- $\pi^0$  background. (a) Diphoton invariant mass distribution, (b) photon transverse momentum distribution.

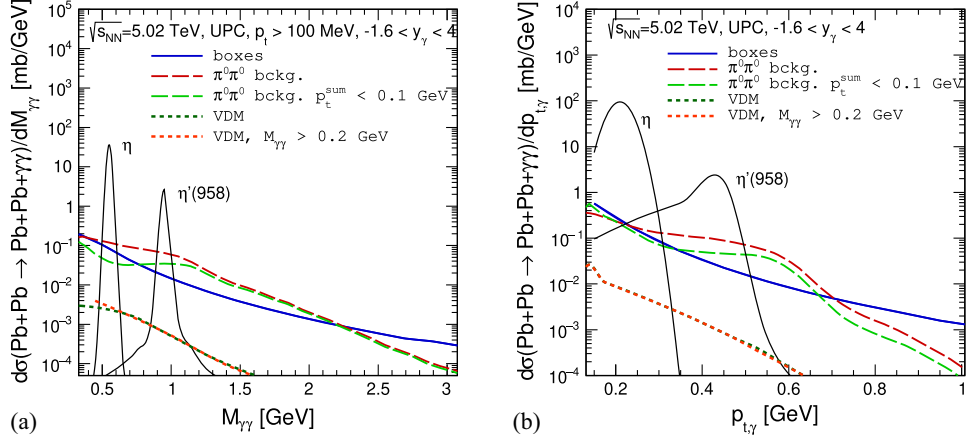


FIG. 22. Prediction for the ALICE 3 experiment for photons:  $p_t > 100$  MeV and photon rapidities  $y_i \in (-1.6, 4)$ . The blue line corresponds to fermionic loops, the red line relates to the double- $\pi^0$  background. (a) Diphoton invariant mass, (b) photon transverse momentum distribution.

In principle, there is an option to leave the FoCal detector [13] when running the ALICE 3 detector. This option will be explored elsewhere.

At somewhat larger  $M_{\gamma\gamma}$  and/or  $p_t$  the background contribution becomes as big as the signal (box) contribution (see Fig. 22). Imposing a cut  $|\vec{p}_{1,t} + \vec{p}_{2,t}| < 0.1$  GeV reduces the background contribution. It can be further reduced by imposing a cut on so-called vector

asymmetry  $A_V$  (see [7]). However, assuming no background constraints, the cross section for this rapidity range is twice as large as the signal contribution, see Table III. A comparison of the total cross sections for the three scenarios shows that the most optimistic scenario is the photon forward detection and  $p_{t,\gamma} = (1 - 50)$  MeV. Here, the double- $\pi^0$  background does not play significant role.

TABLE III. Fermionic box signal contribution versus double- $\pi^0$  background given in  $\mu b$  at PbPb collision energy  $\sqrt{s_{NN}} = 5.02$  TeV, with three considered scenarios of ALICE 3 detector limitations.

Kinematical limitation			$\sigma(\pi^0\pi^0 \text{ bckg}) \mu b$	$\sigma(\text{boxes}) \mu b$
$p_t > 5$ MeV	$E_\gamma > 50$ MeV	$-4 < \eta_\gamma < 4$	112.824	952.590
$p_t > 100$ MeV	$E_\gamma > 50$ MeV	$-1.6 < \eta_\gamma < 4$	159.231	82.682
$p_t = (1-50)$ MeV	$E_\gamma > 50$ MeV	$3 < \eta_\gamma < 5$	105.301	3095.795

## V. CONCLUSIONS

We have discussed different mechanisms of  $\gamma\gamma \rightarrow \gamma\gamma$  scattering such as leptonic/quarkish boxes, double hadronic fluctuations, neutral  $t/u$ -channel pion exchanges, and two-gluon exchanges. Possible effects of the subleading mechanisms have been discussed. The latter contributions turned out difficult to be identified in previous ATLAS and CMS measurements. We have discussed possible interference effect of box and double-hadronic fluctuations for  $\gamma\gamma \rightarrow \gamma\gamma$  scattering.

We have calculated several differential distributions for diphotons in the equivalent photon approximation such as  $d\sigma/dp_t$ ,  $d\sigma/dy$ ,  $d\sigma/dM_{\gamma\gamma}$ ,  $d\sigma/dy_{\text{diff}}$ ,  $d\sigma/dy_1 dy_2$  for  $\text{PbPb} \rightarrow \text{PbPb}\gamma\gamma$ . Imposing cuts on  $y_{\text{diff}}$  and transverse momenta of each of the photons ( $p_t < 0.2$  GeV) or  $M_{\gamma\gamma} > 20$  GeV and cut on transverse momenta of photons we have found regions of the phase space with the dominance of the hadronic excitation of both photons, called in this paper VDM-Regge for brevity. Identification of this mechanism at ALICE 3 would be very interesting and would allow to verify the concept of the VDM-Regge experimentally.

We have also considered the two- $\pi^0$  background, one photon from one  $\pi^0$  and a second photon from the other  $\pi^0$ , which gives a relatively large cross section that could be misidentified as the  $\gamma\gamma \rightarrow \gamma\gamma$  process. Imposing lower cuts on  $|\vec{p}_{1t} + \vec{p}_{2t}|$  or alternatively azimuthal angle between photons eliminates a big part of the unwanted two- $\pi^0$  background but still some contribution at  $M_{\gamma\gamma} \sim 1$  GeV survives.

We have also explored an option to use the planned FoCal detector. When used simultaneously with the ALICE main detector it may allow to study the  $\gamma\gamma \rightarrow \gamma\gamma$  scattering for  $W_{\gamma\gamma} < 1$  GeV, a new unexplored region of the sub-system energies. Therefore we conclude that the measurement of  $\gamma + \gamma \rightarrow \gamma + \gamma$  in a unique region of relatively small

energies and small transverse momenta (much lower than those for ATLAS or CMS) will be possible.

We have also made predictions for the ALICE 3 ( $-4 < y_\gamma < 4$ ) and for a planned special soft photon detector ( $3 < y_\gamma < 5$ ). We have shown that by imposing a cut on  $y_{\text{diff}} = y_1 - y_2$  one can efficiently eliminate the unwanted double  $\pi^0$  background. The soft photon detector can be used to measure the  $\gamma\gamma \rightarrow \gamma\gamma$  scattering at extremely small energies,  $W_{\gamma\gamma} < 0.05$  GeV. Therefore we conclude that the ALICE 3 infrastructure will be an extremely useful to study the  $\gamma\gamma \rightarrow \gamma\gamma$  scattering in a new, not yet explored, domain of energies and transverse momenta. In this domain the double- $\pi^0$  background can to large extent be eliminated.

For photon-photon energies (diphoton invariant masses)  $1 \text{ GeV} < W_{\gamma\gamma} < 2 \text{ GeV}$  the tensor meson exchanges may play an important role (see [10]). They would lead to deviations from the box component. This effect may be difficult to eliminate by imposing cuts on diphoton invariant mass.

In the present calculations we used an equivalent photon approximation in the impact parameter space. In the future one can try to use also so-called Wigner function approach (never used for the diphoton production). This goes, however, beyond the scope of the present exploratory paper.

## ACKNOWLEDGMENTS

This work was partially supported by the Polish National Science Center Grant No. UMO-2018/31/B/ST2/03537 and by the Center for Innovation and Transfer of Natural Sciences and Engineering Knowledge in Rzeszów. We are indebted to Adam Matyja, Jacek Otwinowski and Rainer Schicker for a discussion on ALICE 3 and FoCAL projects.

- 
- [1] L. Doyle, P. Khademi, P. Hilz, A. Sävert, G. Schäfer, J. Schreiber, and M. Zepf, *New J. Phys.* **24**, 025003 (2022).
  - [2] D. d'Enterria and G.G. da Silveira, *Phys. Rev. Lett.* **111**, 080405 (2013); **116**, 129901(E) (2016).
  - [3] M. Aaboud *et al.* (ATLAS Collaboration), *Nat. Phys.* **13**, 852 (2017).
  - [4] A. M. Sirunyan *et al.* (CMS Collaboration), *Phys. Lett. B* **797**, 134826 (2019).
  - [5] G. Aad *et al.* (ATLAS Collaboration), *Phys. Rev. Lett.* **123**, 052001 (2019).
  - [6] G. Aad *et al.* (ATLAS Collaboration), *J. High Energy Phys.* **03** (2021) 243; **11** (2021) 050(E).
  - [7] M. Klusek-Gawenda, R. McNulty, R. Schicker, and A. Szczurek, *Phys. Rev. D* **99**, 093013 (2019).
  - [8] M. Klusek-Gawenda, P. Lebedowicz, and A. Szczurek, *Phys. Rev. C* **93**, 044907 (2016).
  - [9] M. Klusek-Gawenda, W. Schäfer, and A. Szczurek, *Phys. Lett. B* **761**, 399 (2016).
  - [10] P. Lebedowicz and A. Szczurek, *Phys. Lett. B* **772**, 330 (2017).
  - [11] R. O. Coelho, V.P. Gonçalves, D.E. Martins, and M. Rangel, *Eur. Phys. J. C* **80**, 488 (2020).
  - [12] C. Baldenegro, S. Fichet, G. von Gersdorff, and C. Royon, *J. High Energy Phys.* **06** (2018) 131.
  - [13] C. Loizides, W. Riegler *et al.* (ALICE Collaboration), CERN Document Server (2020), [arXiv:2211.02491](https://arxiv.org/abs/2211.02491).
  - [14] L. Musa, W. Riegler *et al.* (ALICE Collaboration), CERN Document Server (2022), [arXiv:2211.02491](https://arxiv.org/abs/2211.02491).

- [15] P. Lebiedowicz and A. Szczurek, *Phys. Lett. B* **772**, 330 (2017).
- [16] A. Szczurek, N. N. Nikolaev, and J. Speth, *Phys. Rev. C* **66**, 055206 (2002).
- [17] A. Szczurek and J. Speth, *Nucl. Phys. A* **728**, 182 (2003).
- [18] M. M. Brisudová, L. Burakovsky, and T. Goldman, *Phys. Rev. D* **61**, 054013 (2000).
- [19] M. M. Brisudova, L. Burakovsky, T. Goldman, and A. Szczepaniak, *Phys. Rev. D* **67**, 094016 (2003).
- [20] M. Klusek-Gawenda and A. Szczurek, *Phys. Rev. C* **82**, 014904 (2010).
- [21] M. Klusek-Gawenda and A. Szczurek, *Phys. Rev. C* **87**, 054908 (2013).
- [22] M. Klusek-Gawenda and A. Szczurek, *Phys. Rev. C* **87**, 054908 (2013).
- [23] L. A. Harland-Lang, M. Tasevsky, V. A. Khoze, and M. G. Ryskin, *Eur. Phys. J. C* **80**, 925 (2020).
- [24] G. K. Krintiras, I. Grabowska-Bold, M. Klusek-Gawenda, E. Chapon, R. Chudasama, and R. Granier de Cassagnac, *Acta Phys. Pol. B Proc. Suppl.* **16**, 123 (2023).